Article

Ultraviolet-Visible-Near Infrared Broadband Photodetector Based on Electronspun Disorder ZnO Nanowires/Ge Quantum Dots Hybrid Structure

Jie You [1], Yichi Zhang [1], Maolong Yang [1], Bo Wang [1], Huiyong Hu [1], Zimu Wang [2], Jinze Li [3], Hao Sun [3,*] and Liming Wang [1,*]

[1] Wide Bandgap Semiconductor Technology Disciplines State Key Laboratory, School of Microelectronics, Xidian University, Xi'an 710071, China; jyou@stu.xidian.edu.cn (J.Y.); yc_zhang@stu.xidian.edu.cn (Y.Z.); lmyang@stu.xidian.edu.cn (M.Y.); bowang2020@stu.xidian.edu.cn (B.W.); huhy@xidian.edu.cn (H.H.)
[2] College of Engineering, Unviersity of California, Davis, CA 95616, USA; zmuwang@ucdavis.edu
[3] School of Physics and Optoelectronic Engineering, Xidian University, Xi'an 710071, China; jinze_lee@vip.163.com
* Correspondence: hsun@xidian.edu.cn (H.S.); lmwang@xidian.edu.cn (L.W.); Tel.: +86-181-9248-6131 (H.S.); +86-136-7162-3619 (L.W.)

Abstract: Ultraviolet-visible-near infrared broadband photodetectors have significant prospects in many fields such as image sensing, communication, chemical sensing, and day and nighttime surveillance. Hybrid one-dimensional (1D) and zero-dimensional (0D) materials are attractive for broadband-responsive photodetectors since its unique charges transfer characteristics and facile fabrication processes. Herein, a Si/ZnO nanowires/Ge quantum dots photodetector has been constructed via processes that combined electrospinning and spin-coating methods. A broadband response behavior from ultraviolet to near-infrared (from 250 to 1550 nm) is observed. The responsivity of the hybrid structure increases around three times from 550 to 1100 nm compared with the pure Si photodetector. Moreover, when the photodetector is illuminated by a light source exceeding 1100 nm, such as 1310 and 1550 nm, there is also a significant photoresponse. Additionally, the ZnO NWs/Ge quantum dots heterostructure is expected to be used in flexible substrates, which benefits from electrospinning and spin-coating processes. The strategy that combines 1D ZnO NWs and 0D solution-processed Ge QDs nanostructures may open a new avenue for flexible and broadband photodetector.

Keywords: hybrid structure; broadband photodetection; electrospinning; optoelectronic

1. Introduction

Silicon (Si)-based photodetectors (PDs) with a broad spectral response from the ultraviolet (UV)-visible (vis) to the near infrared (NIR) are fast becoming a key component in various applications, including environmental monitoring, chemical/biological analysis, optical communication, and integrated optoelectronics [1]. However, it is impossible to realize these broadband PDs based on Si itself as light-sensitive layer due to the ultra-low photoresponse in the ultraviolet (<400 nm) and infrared (>1100 nm) regions. The former originates from the high reflection coefficient and shallow penetration depth of ultraviolet light (<400 nm) in Si, while the latter is attributed to the cutoff wavelength of 1100 nm related to the 1.12 eV band gap of Si [2–4]. These fundamental shortcomings, however, can be overcome by integration other semiconductors with Si to extending the detection range of Si-based PDs [5–7].

Over the past few decades, zinc oxide (ZnO) has emerged as an ideal candidate for UV PDs because of its unique properties, including the wide bandgap (3.4 eV), high electron mobility, simple synthesis process, and large exciting energy (60 meV) [8]. Thanks

to the anisotropic transmission characteristics and the high surface-to-volume ratio, one-dimensional (1D) ZnO nanowires (NWs) can exhibit more excellent photoelectric performances compared with bulk ZnO [9]. A variety of growth techniques, including chemical vapor deposition (CVD), electrospinning, and hydrothermal processes, have been investigated for growing ZnO NWs on Si substrates [10–12]. Among them, electrospinning is the preferential method due to its facile and low-cost fabrication, as well as its versatile applications. In this case, ZnO NWs/Si PDs can exhibit a unique photoresponse performance from UV to NIR range (ACS Appl. Electron. Mater. 2020, 2, 2819–2828) [13].

In order to rise the detection properties of ZnO NWs/Si PDs in the infrared range (850–1800 nm), Ge is a promising alternative because of the narrow bandgap (0.67 eV), the highest hole mobility of all of the known semiconductor materials, and the compatibility with the CMOS manufacturing process [14]. In particular, Ge quantum dots (QDs) have outstanding photoelectric performance due to their enhanced quantum efficiency associated with the quantum confinement effect [15]. The bandgap of Ge QDs also can be modified by the size of the QDs, which results in an adjustable cutoff wavelength of the PD [16]. At the same time, the typical methods for growth of Ge QDs, such as molecular beam epitaxy (MBE) and CVD, require extremely complicated technological processes, high-cost experimental facilities, and a high-temperature environment, which have limited applications [17,18]. By contrast, chemical synthesis provides a powerful and facile path for achieving the size-controlled QDs, and these QDs can be easily transferred to various substrates [19]. Therefore, compounding Ge QDs into ZnO NWs/Si PD has great potential for realizing the broadband detection from the UV-vis to the NIR [6,12,15]. However, the related experimental result on the photodetection performance is rarely reported.

In this paper, we demonstrate a broadband Si-based PD by integration ZnO NWs and Ge QDs with Si substrate. The morphologies, structure, and photoresponse properties of the device are characterized in detail. A broadband response behavior from UV to NIR (from 250 to 1550 nm) is observed. The related mechanisms are discussed based on the energy band structure. Our results shed new light on the broadband Si-based PD as well as other innovative flexible optoelectronic devices.

2. Materials and Methods

Fabrication of ZnO NWs: ZnO NWs were fabricated on Si substrate via an electrospinning method. The gel of zinc acetate/polyvinylpyrrolidone (PVP) was used as the precursor. Firstly, 1.0 g of $Zn(NO_3)_2 \cdot 6H_2O$ and 2 g PVP (Mn = 1,300,000) was dissolved in 12 mL of *N,N*-dimethylformamide (DMF) solution, and then stirred for 12 h at 30 °C to form a uniform solution. After that, the precursor solution was transferred into a syringe with a metal needle. The injected out rate was set at 0.5 mL·h^{-1}, and a high voltage of 18 kV was applied to the syringe needle. In this way, The $Zn(NO_3)_2$/PVP nanofibers were obtained on the Si substrate. Then, the nanofibers were annealed in air at a temperature of 500 °C for 1 h at the rate of 5 °C/min, so disordered ZnO nanofibers were obtained [20].

Synthesis of Ge QDs: Ge QDs were prepared by the water phase method. Firstly, 34 g $NaBH_4$ was added into 100 mL icy cold distilled water and stirred to form 0.32 mol·L^{-1} uniform solution. In the meanwhile, 0.26 g GeO_2 powder and 0.01 g PVP (Mn = 58,000) were dissolved into 10 mL 0.15 mol·L^{-1} NaOH solution, and then the PH of the solution was adjusted by acetic acid to be 7. Afterwards, the above two solutions were mixed in a beaker and followed by a water bath at 60 °C for 3 h. Then, the dark brown solution was centrifuged at 3000 rpm speed for 5 min, after that the precipitate was separated and transferred to a vacuum drying-off oven to obtain dark-blown powders. Finally, the powders were annealed in vacuum at 600 °C for 1 h at the rate of 5 °C/min and distributed in deionized water [6].

Device Fabrication: To obtain the ZnO NWs/Ge QDs hybrid photodetectors, firstly, Au arrays with a period of 2 mm and a diameter of 1 mm were deposited onto the Si substrate as the metal contact. Afterwards, ZnO nanofibers were deposited on the Si substrate via charge transfer paths. Then, the Ge QDs layer was distributed onto the ZnO nanofibers

which coated Si substrate. In brief, 5 mg mL^{-1} Ge QDs solution was spin-coated on the Si substrate at 1000 rpm for 30 s and dried in a hot plate at 50 °C for 2 min. The spin-coating with drying treatment was repeated three times to ensure that abundant Ge QDs were attached to the ZnO NWs.

Characterization and measurements of materials: The morphology of annealed ZnO NWs was characterized by a field-emission scanning electron microscope (BX51, OLYMPUS). The crystal quality of ZnO NWs and Ge QDs was characterized with an X-ray diffractometer (XRD, D/MAX-III-B-40KV, Cu Kα radiation, λ = 0.15418 nm). TEM (JEM 2100, JEOL) and X-ray EDS were used to characterize the microstructure and elementary composition of ZnO NWs. The luminescence is analyzed with a monochromator (Omni-λ500, Zolix Instruments Co, Xi'an, China) and detected with an extended InGaAs photodetector using the standard lock-in technique. The excitation source is a 532 nm line of a solid state laser, which has a spot of ~2 mm in diameter.

Photodetecting Measurements for Devices: The photoelectronic characteristics of the photodetector were measured using a Keithley 4200-SCS semiconductor parameter analyzer and a probe station. Additionally, a tungsten halogen lamp (0.3–2.5 μm, Gloria-T250A, Zolix instruments) was used as a broadband light source during the response spectra measurements. This broadband light was initially monochromatized by using a monochromator (Omni-λ300i, Zolix Instruments), whereupon the monochromatic light was coupled into a multi-mode optical fiber and ultimately shined on the device.

3. Results and Discussion

3.1. The Morphology and Structure of ZnO NWs/Ge QDs

Fabrication of Si-based broadband PD by integration ZnO NWs and Ge QDs with Si substrate is schematically depicted in Figure 1. The nanofibers were randomly distributed between two separated gold electrodes under the electrostatic force, and ZnO NWs were then formed after 500 °C annealing in air as shown in Figure 1a. In order to incorporating Ge QDs into the sample, Ge QDs solution (5 mg/mL) fabricated by chemical synthesis method was spun onto the ZnO NWs. Additionally, a thin film of Ge QDs on the surface of ZnO NWs was obtained via a spin-coating process (Figure 1b).
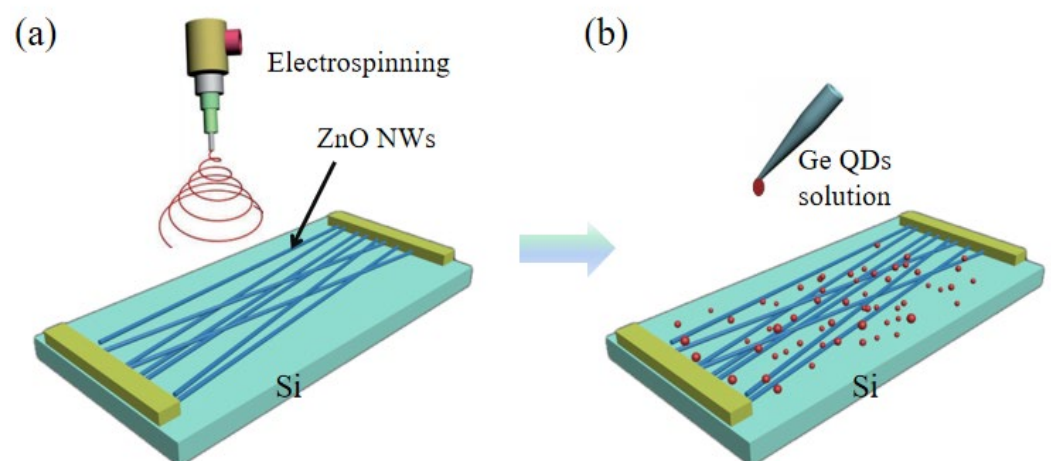

Figure 1. Schematic illustration of fabricating for Si/ZnO NWs/Ge QDs broadband PD. (**a**) A schematic view for electrospinning ZnO NWs. (**b**) A schematic spin-coating Ge QDs on ZnO NWs.

Figure 2a,b show the scanning electron microscope (SEM) of ZnO at different magnifications. The average diameter of randomly distributed ZnO NWs is 100 nm, and the density is directly proportional to electrospinning time. There are around five ZnO NWs layers stacked longitudinally in the SEM imagine at a large magnification. In sequence, the thickness of the ZnO film is estimated as 500 nm. The element information was given in the energy dispersive X-ray (EDS) analysis spectrum shown in Figure 2c, which proves the primary composition of ZnO and Si because of the existence of Si, oxygen, and Zn elements.

Accordingly, the averaged element weights are 39.46%, 36.48%, and 24.06% for Si, oxygen, and Zn, respectively. In order to further analyze the crystal structures of ZnO, the X-ray diffraction (XRD) results of the sample was displayed in Figure 2d. A high crystal quality of ZnO NWs is proved by the sharp peaks [21].
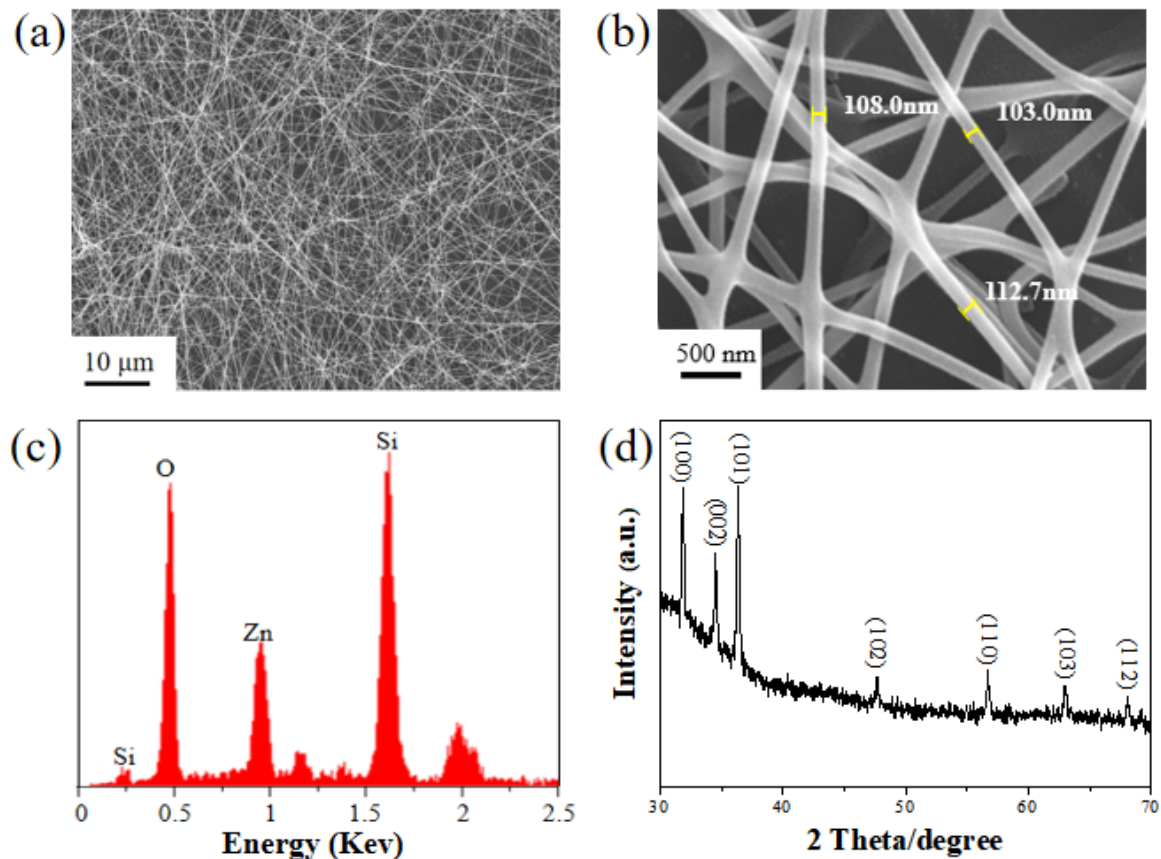

Figure 2. Morphology and microstructure studies of the ZnO NWs. (**a**,**b**) SEM images of ZnO NWs at different magnifications. (**c**) EDS spectrum of ZnO NWs. (**d**) XRD spectrum of annealed ZnO NWs.

Figure 3a displays the XRD results of Ge QDs before and after annealing at 600 °C for 1 h in vacuum. The spectrum of the unannealed Ge QDs consists of two broadening diffraction peaks. By contrast, the XRD results of annealed Ge QDs demonstrates intensive and sharp diffraction peaks, which are in good agreement with the standard XRD pdf card of # 65-0333. This phenomenon indicates that the crystal quality of Ge QDs can be significantly improved by the annealing process [22]. Figure 3b shows the TEM image of Ge QDs after the oxidation reacting and annealing, and the Ge QDs as well as GeO_xH_y shell are exhibited in Figure 3b. The vague boundary contours of Ge QDs and GeO_xH_y shells are marked as dotted lines. The average diameter of Ge QDs is 8 nm; in this case, the efficient quantum confinement effect will be supported in the Ge QDs. Figure 3c shows the photoluminescence (PL) spectra at room temperature, which were measured to estimate the band-gap energy of Ge QDs and bulk Ge, and the value is 0.8 and 0.67 eV for Ge QDs and bulk Ge, respectively. As compared to the bulk Ge, a blue shift in emission peak is observed in the PL spectra of Ge QDs, which is ascribed to the strong quantum confinement effect [23,24]. Additionally, the PL spectrum of Ge QDs further proves that the material can absorb infrared light (1300–1800 nm) efficiently.
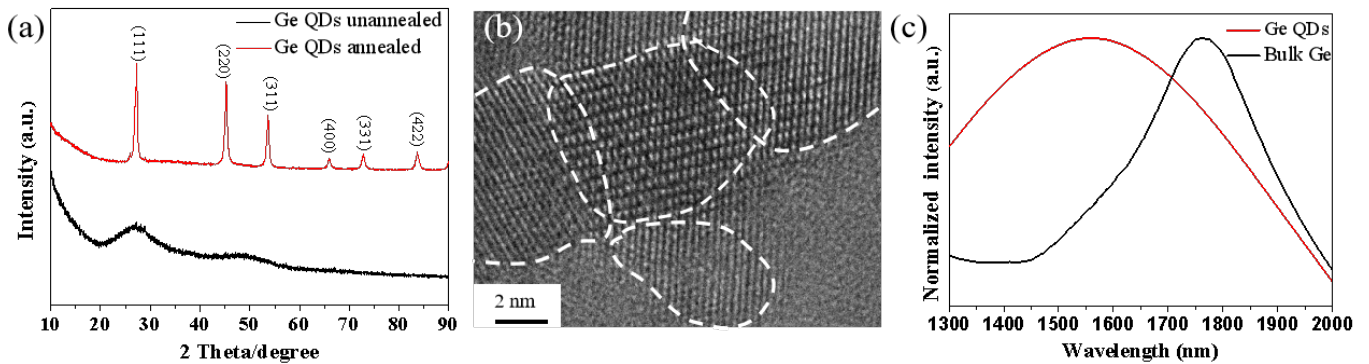
Figure 3. (**a**) XRD results of Ge QDs before and after annealing. (**b**) TEM image of annealed Ge QDs. (**c**) The PL spectra of annealed Ge QDs and bulk Ge wafer.

3.2. Optoelectronic Properties of ZnO NWs/Ge QDs Hybrid Structure

The optoelectrical characteristics are performed to verify the photodetection performance of Si/ZnO NWs/Ge QDs PD. Figure 4a shows the I–V curves of the device measured in the dark and under UV-NIR light illumination, and the optical powers are 2.3, 3.7, 7.9, 16, and 23.5 mW for 254, 365, 532, 1310, and 1550 nm, respectively. It should be noticed that the photocurrents increase dramatically under illuminated by UV-Vis light, and the high photo-to-dark current ratio allows a high signal-to-noise and is beneficial to practical applications. There is an obvious photoresponse when the photodetector is illuminated by 1310 and 1550 nm lasers, respectively. However, the responses are smaller than those illuminated by UV and vis light, and the details will be discussed below. To further analyze the characteristics of the devices, pure Si wafer as PD and Si/ZnO NWs/Ge QDs PD are illuminated under UV (254 nm) and NIR light (1310 nm), as shown in Figure 4b,c respectively. The photocurrent of Si/ZnO NWs/Ge QDs PD is almost four times larger than that of Si photodetector under 254 nm light illumination, which is attributed to the separation of the charges by ZnO NWs/Si heterojunction and the enhanced absorption coefficient in the UV band [25,26]. Before and after 1310 nm light illumination, the I–V curves of Si PD are overlapped, which indicates that there is no photoresponse of Si PD in this region. Such a feature originates from the limited cutoff wavelength (1100 nm) due to the large band gap (1.12 eV). By contrast, the Si/ZnO NWs/Ge QDs PD exhibits a conspicuous photoresponse under 1310 nm light illumination as shown in Figure 4c. This phenomenon demonstrates Ge QDs can extend the detection range in the NIR region, which plays a vital role in the broadband Si/ZnO NWs/Ge QDs PD. Figure 4d shows that the responsivity of the Si/ZnO NWs/Ge QDs and pure Si PD depends on the wavelength of incident light at −8 V reverse voltage, which can be calculated by [27,28],

$$R(A \cdot W^{-1}) = \frac{I_p}{P_{in}} \tag{1}$$

where I_P is photocurrent, and P_{in} is the incident optical power. The incident optical power is obtained by an optical power meter with an InGaAs sensor. Compared with pure Si PD, about a 300% enhancement in responsivity of Si/ZnO NWs/Ge QDs PD is observed in the wavelength range of 550 to 1100 nm. Meanwhile, the detection waveband of the hybrid device has been extended to the ultraviolet and near-infrared region of longer than 1.1 μm. As shown in the Table 1, we have compared detection wavelength and responsivity of our PD with literatures, and the Si/ZnO NWs/Ge QDs hybrid structure shows relatively high performance.
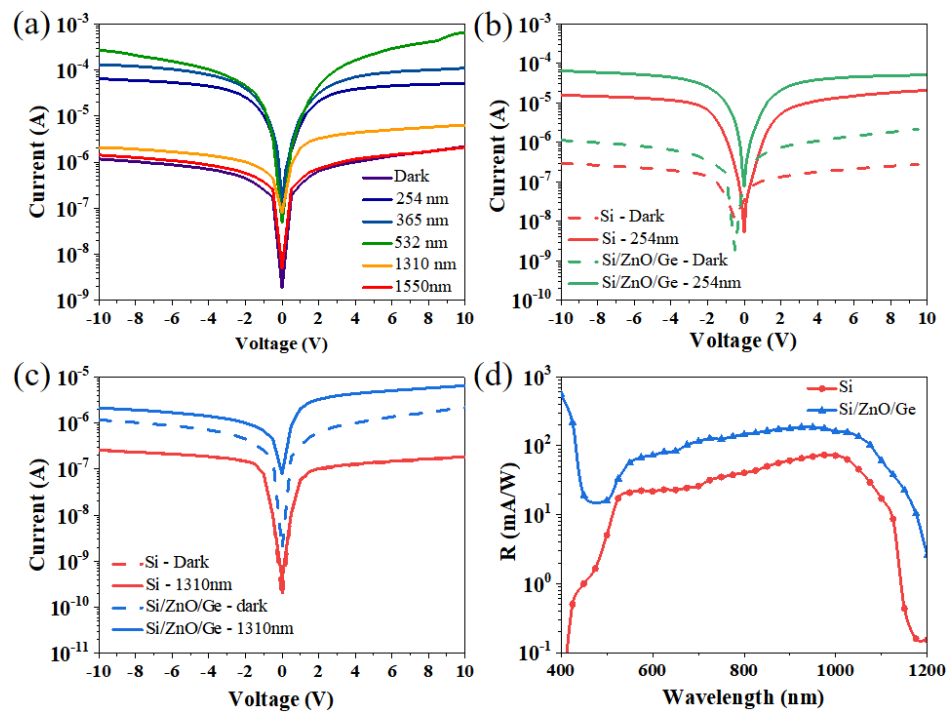
Figure 4. (**a**) I-V characteristics of the Si/ZnO NWs/Ge QDs PD in the dark and under UV-vis-Nir light illuminations (the optical powers are 2.3, 3.7, 7.9, 16, and 23.5 mW for 254, 365, 532, 1310, and 1550 nm, respectively). I-V characteristics of Si and Si/ZnO NWs/Ge QDs PD under 254 nm (**b**) or 1310 nm (**c**) light illumination. (**d**) The responsivity of Si and hybrid PD as a function of wavelength of illuminated light at −8 V reverse voltage.

Table 1. The performances of Si/ZnO/Ge PD and perviously reported hybrid PDs.

PDs	Wavelength (nm)	Responsivity (mA/W)	Ref.
Si/ZnO/Ge	254–1550	172 (880 nm, −8 V)	This work
Si/ZnO	365–1550	5.9 (880 nm, 0 V)	[13]
ZnO/perovskite	350–850	670 (740 nm, 1 V)	[12]
ZnO/PbS QDs	300–1000	11 (900 nm, 10 V)	[20]
Si/Ge QDs	808–1550	1.5 (1550 nm, 5 V)	[15]

To elucidate the mechanism of unique photoresponse features of Si/ZnO NWs/Ge QDs PD under UV and NIR light illumination, the energy band diagrams of the structure are analyzed as shown in Figure 5a,b. Electron affinities of Si and ZnO are χ(Si) = 4.04 eV and χ(ZnO) = 4.35 eV, respectively [29]. The band-gaps of Si and ZnO are taken as E_g(Si) = 1.12 eV and E_g(ZnO) = 3.37 eV, respectively. In consequence, the conduction band offset for electrons is ΔE_c = χ(ZnO) − χ(Si) = 0.31 eV, whereas that for holes is ΔE_c = χ(ZnO) − χ(Si) + E_g(ZnO) − E_g(Si) = 2.56 eV. Therefore, type-II energy band alignment is obtained at the interface of P-Si and N-ZnO, as shown in Figure 5a. Owing to this special energy band alignment, electrons will move to the ZnO side and holes will move to Si side due to the internal field after the generation of electron-hole pairs in ZnO NWs and Si under UV and Vis light illumination. This mechanism will facilitate the spatial separation of the photogenerated carriers and result in a larger photocurrent compared with pure Si

photodetector [20]. When the hybrid PD is illuminated by NIR light, photogenerated carriers in Ge QDs need to tunnel through the GeO_xH_y shell when transferring to ZnO NWs under the electric field force (Figure 5b) [6]. In this case, the photoresponse in NIR range of the hybrid PD can be significantly enhanced, as shown in Figure 4c. However, few photogenerated carriers are collected by electrodes due to the difficulty of tunneling effect and the probability of tunneling is reduced with longer wavelengths in NIR region. Therefore, there is a slight performance improvement of photodetector illuminated under 1550 nm light.
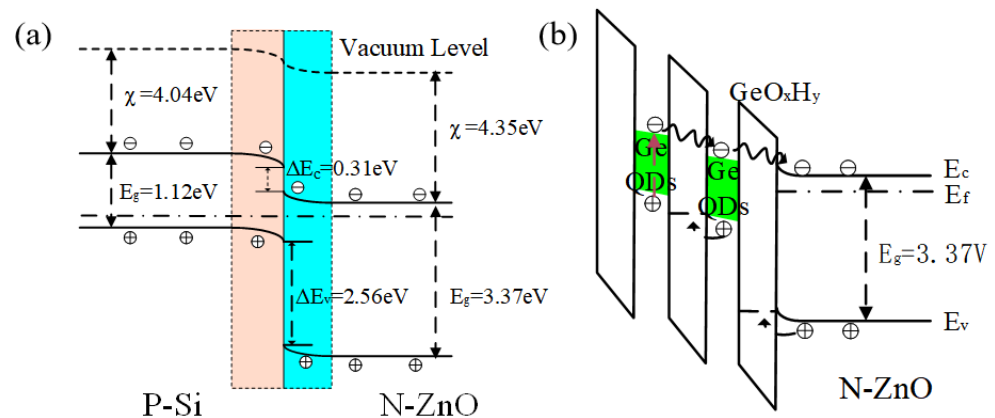

Figure 5. Energy band diagram of Si/ZnO NWs' (**a**) and ZnO NWs/Ge QDs' (**b**) hybridization structure under UV and NIR light illumination, respectively.

4. Conclusions

In summary, a broadband Si/ZnO NWs/Ge QDs PD based on facile electrospinning and spin-coating processes has been successfully designed and fabricated. This hybrid photodetector demonstrates a wider response ranging from UV to NIR with significantly enhanced responsivity from 254 to 1550 nm compared to pure Si. The significantly improved performance of the hybrid photodetector is attributed to the fact that photogenerated charges are separated efficiently. At the same time, when the PD is illuminated by a light source exceeding 1100 nm, such as 1310 and 1550 nm, there is also a significant photoresponse. However, the detection properties at NIR is weaker than that at UV and Vis range due to a difficult photogenerated carriers transport between Ge QDs and ZnO NWs. Because the Ge QDs are completely enclosed by the dielectric GeOxHy shell, now that the fundamental boundaries of broadband Si-based PD have been removed, If the transport properties of carriers between Ge QDs and ZnO NWs can be further enhanced, the strategy of integration ZnO NWs and Ge QDs on Si substrate may provide a promising route toward the applications of Si-based PD with wide-range response and innovative flexible devices.

Author Contributions: Investigation, Z.W., Y.Z., M.Y., B.W., J.L. and H.S.; writing—original draft preparation, J.Y.; Supervision, L.W. and H.H. All authors have read and agreed to the published version of the manuscript.

Institutional Review Board Statement: Not applicable.

Informed Consent Statement: Not applicable.

Data Availability Statement: The data presented in this study are available on request from the corresponding author.

Conflicts of Interest: The authors declare no conflict of interest.

References

1. Zhao, Z.; Xu, C.; Niu, L.; Zhang, X.; Zhang, F. Recent Progress on Broadband Organic Photodetectors and their Applications. *Laser Photonics Rev.* **2020**, *14*, 2000262. [CrossRef]
2. El-Amir, A.A.; Ohsawa, T.; Ishii, S.; Imura, M.; Liao, M.; Fu, X.; Segawa, H.; Sakaguchi, I.; Nagao, T.; Shimamura, K.; et al. Silicon-compatible Mg2Si/Si n-p photodiodes with high room temperature infrared responsivity. *Mater. Sci. Semicond. Process.* **2019**, *102*, 104577. [CrossRef]
3. Naderi, N.; Hashim, M. Porous-shaped silicon carbide ultraviolet photodetectors on porous silicon substrates. *J. Alloy. Compd.* **2013**, *552*, 356–362. [CrossRef]
4. Wan, X.; Xu, Y.; Guo, H.; Shehzad, K.; Ali, A.; Liu, Y.; Yang, J.; Dai, D.; Lin, C.-T.; Liu, L.; et al. A self-powered high-performance graphene/silicon ultraviolet photodetector with ultra-shallow junction: Breaking the limit of silicon? *Npj 2D Mater. Appl.* **2017**, *1*, 4. [CrossRef]
5. Tsai, D.-S.; Lin, C.-A.; Lien, W.-C.; Chang, H.-C.; Wang, Y.-L.; He, J.-H. Ultra-High-Responsivity Broadband Detection of Si Metal–Semiconductor–Metal Schottky Photodetectors Improved by ZnO Nanorod Arrays. *ACS Nano* **2011**, *5*, 7748–7753. [CrossRef]
6. Liu, X.; Ji, X.; Liu, M.; Liu, N.; Tao, Z.; Dai, Q.; Wei, L.; Li, C.; Zhang, X.; Wang, B. High-Performance Ge Quantum Dot Decorated Graphene/Zinc-Oxide Heterostructure Infrared Photodetector. *ACS Appl. Mater. Interfaces* **2015**, *7*, 2452–2458. [CrossRef] [PubMed]
7. Song, W.; Wang, X.; Chen, H.; Guo, D.; Qi, M.; Wang, H.; Luo, X.; Luo, X.; Li, G.; Li, S. High-performance self-powered UV-Vis-NIR photodetectors based on horizontally aligned GaN microwire array/Si heterojunctions. *J. Mater. Chem. C* **2017**, *5*, 11551–11558. [CrossRef]
8. Shaikh, S.K.; Inamdar, S.I.; Ganbavle, V.V.; Rajpure, K.Y. Chemical bath deposited ZnO thin film based UV photo-conductive detector. *J. Alloy. Compd.* **2016**, *664*, 242–249. [CrossRef]
9. Redeker, N.D.; Danesh, C.D.; Ding, Y.; Zhang, S. Anisotropic core–shell nanocomposites by direct covalent attachment of a side-functionalized poly(3-hexylthiophene) onto ZnO nanowires. *Polymer* **2013**, *54*, 7004–7008. [CrossRef]
10. Podrezova, L.V.; Porro, S.; Cauda, V.; Fontana, M.; Cicero, G. Comparison between ZnO nanowires grown by chemical vapor deposition and hydrothermal synthesis. *Appl. Phys. A* **2013**, *113*, 623–632. [CrossRef]
11. Wu, W.-Y.; Ting, J.-M.; Huang, P.-J. Electrospun ZnO Nanowires as Gas Sensors for Ethanol Detection. *Nanoscale Res. Lett.* **2009**, *4*, 513–517. [CrossRef]
12. Cao, F.; Tian, W.; Gu, B.; Ma, Y.; Lu, H.; Li, L. High-performance UV–vis photodetectors based on electrospun ZnO nanofiber-solution processed perovskite hybrid structures. *Nano Res.* **2017**, *10*, 2244–2256. [CrossRef]
13. Chatzigiannakis, G.; Jaros, A.; Leturcq, R.; Jungclaus, J.; Voss, T.; Gardelis, S.; Kandyla, M. Laser-Microstructured ZnO/p-Si Photodetector with Enhanced and Broadband Responsivity across the Ultraviolet–Visible–Near-Infrared Range. *ACS Appl. Electron. Mater.* **2020**, *2*, 2819–2828. [CrossRef]
14. Rigo, R.T.; Balestra, S.R.G.; Hamad, S.; Bueno-Perez, R.; Ruiz-Salvador, A.R.; Calero, S.; Camblor, M.A. The Si–Ge substitutional series in the chiral STW zeolite structure type. *J. Mater. Chem. A* **2018**, *6*, 15110–15122. [CrossRef]
15. Zhao, Y.; Li, L.; Liu, S.; Wang, J.; Xu, J.; Shi, Y.; Chen, K.; Roca, I.C.P.; Yu, L. Germanium quantum dot infrared photo-detectors addressed by self-aligned silicon nanowire electrodes. *Nanotechnology* **2020**, *31*, 145602. [CrossRef] [PubMed]
16. Raciti, R.; Bahariqushchi, R.; Summonte, C.; Aydinli, A.; Terrasi, A.; Mirabella, S. Optical bandgap of semiconductor nanostructures: Methods for experimental data analysis. *J. Appl. Phys.* **2017**, *121*, 234304. [CrossRef]
17. Chen, P.; Pei, Z.; Peng, Y.; Lee, S.; Tsai, M.-J. Boron mediation on the growth of Ge quantum dots on Si (100) by ultra high vacuum chemical vapor deposition system. *Mater. Sci. Eng. B* **2004**, *108*, 213–218. [CrossRef]
18. Huo, Y.; Lin, H.; Chen, R.; Rong, Y.; Kamins, T.I.; Harris, J.S. MBE growth of tensile-strained Ge quantum wells and quantum dots. *Front. Optoelectron.* **2012**, *5*, 112–116. [CrossRef]
19. Prabakar, S.; Shiohara, A.; Hanada, S.; Fujioka, K.; Yamamoto, K.; Tilley, R.D. Size Controlled Synthesis of Germanium Nanocrystals by Hydride Reducing Agents and Their Biological Applications. *Chem. Mater.* **2009**, *22*, 482–486. [CrossRef]
20. Zheng, Z.; Gan, L.; Zhang, J.; Zhuge, F.; Zhai, T. An Enhanced UV-Vis-NIR an d Flexible Photodetector Based on Electrospun ZnO Nanowire Array/PbS Quantum Dots Film Heterostructure. *Adv. Sci.* **2017**, *4*, 1600316. [CrossRef]
21. Li, S.Y.; Lin, P.; Lee, C.Y.; Tseng, T.Y.; Huang, C.J. Effect of Sn dopant on the properties of ZnO nanowires. *J. Phys. D Appl. Phys.* **2004**, *37*, 2274–2282. [CrossRef]
22. Chou, N.H.; Oyler, K.D.; Motl, N.E.; Schaak, R.E. Colloidal Synthesis of Germanium Nanocrystals Using Room-Temperature Benchtop Chemistry. *Chem. Mater.* **2009**, *21*, 4105–4107. [CrossRef]
23. Ren, S.Y. Quantum confinement in semiconductor Ge quantum dots. *Solid State Commun.* **1997**, *102*, 479–484. [CrossRef]
24. Chang, J.; Liao, P.H.; Chien, C.Y.; Hsu, J.C.; Hung, M.T.; Chang, H.T.; Lee, S.W.; Chen, W.Y.; Hsu, T.M.; George, T.; et al. Matrix and quantum confinement effects on optical and thermal properties of Ge quantum dots. *J. Phys. D Appl. Phys.* **2012**, *45*. [CrossRef]
25. Chen, C.-H.; Chang, S.-J.; Chang, S.-P.; Li, M.-J.; Chen, I.C.; Hsueh, T.-J.; Hsu, C.-L. Novel fabrication of UV photodetector based on ZnO nanowire/p-GaN heterojunction. *Chem. Phys. Lett.* **2009**, *476*, 69–72. [CrossRef]
26. Ouyang, B.; Zhao, H.; Wang, Z.L.; Yang, Y. Dual-polarity response in self-powered ZnO NWs/Sb2Se3 film heterojunction photodetector array for optical communication. *Nano Energy* **2020**, *68*, 104312. [CrossRef]

27. Zhang, Y.; Huang, P.; Guo, J.; Shi, R.; Huang, W.; Shi, Z.; Wu, L.; Zhang, F.; Gao, L.; Li, C.; et al. Graphdiyne-Based Flexible Photodetectors with High Responsivity and Detectivity. *Adv. Mater.* **2020**, *32*, e2001082. [CrossRef]

28. Youngblood, N.; Chen, C.; Koester, S.J.; Li, M. Waveguide-integrated black phosphorus photodetector with high re-sponsivity and low dark current. *Nat. Photonics* **2015**, *9*, 247–252. [CrossRef]

29. Xu, J.; Jia, Z.; Zhang, N.; Ren, T. Influence of La and Mn dopants on the current-voltage characteristics of BiFeO3/ZnO heterojunction. *J. Appl. Phys.* **2012**, *111*, 051611. [CrossRef]